Amorphization of crystalline Si due to heavy and light ion irradiation

P. D. Edmondson,[1,a)] D. J. Riley,[1] R. C. Birtcher,[2] and S. E. Donnelly[1]
[1]*Institute for Materials Research, University of Salford, Manchester M5 4WT, United Kingdom*
[2]*Materials Science Division, Argonne National Laboratory, Argonne, Illinois 60439, USA*

(Received 24 October 2008; accepted 9 July 2009; published online 19 August 2009)

The formation of amorphous silicon in crystalline silicon by bombardment with light (Si) and heavy (Xe) ions has been investigated by transmission electron microscopy with *in situ* ion irradiation. Experiments have been carried out at room temperature and low temperature (50 K) and the results are compared to a simple numerical model for amorphization. The results indicate that the amorphization mechanisms for both irradiations are heterogeneous in nature and that numerous overlaps of the collision cascade are generally required to render the crystal amorphous. Following from this, the nature of the material within the confines of collision cascades will be discussed and it will be shown that the individual cascade volume is not necessarily amorphous as previously described in the scientific literature but contains varying degrees of damage depending on the energy deposited within the cascade. © *2009 American Institute of Physics*. [DOI: 10.1063/1.3195081]

I. INTRODUCTION

Current-day microelectronics are generally produced through a four stage process comprising of material preparation, crystal growth and wafer preparation, wafer fabrication, and packaging. In the fabrication stage, the wafer must undergo many processing steps—sometimes above 100. These steps include mask etching, doping, and annealing of the wafers. The doping step of fabrication is generally performed through the process of ion implantation.

During ion implantation, the incoming energetic ion causes damage to the lattice through a series of collisions with the atoms of the crystal. As the incoming ion loses its energy, a collision cascade is formed along the track of the ion. Under situations where the mean free path of the displacing collisions approaches the interatomic spacing, small highly perturbed regions can be formed within which the mean kinetic energy of the target atoms may be increased by several eV—this is the displacement spike.[1] As the kinetic energy deposited by the spike begins to dissipate, localized melting in the spike region may occur. This is known as the thermal spike. The molten material within the spike volume is then rapidly quenched and this may lead to a freezing in of a liquidlike distribution. Although the thermal spike is a subject of much controversy, the work of Donnelly and Birtcher has shown the existence of thermal spikes in metals.[2]

During the thermal spike phase, the energy in the cascade volume begins to spread out and defects may migrate and interact and agglomerate to form more stable defect complexes. After the thermal spike and its associated relaxation phase have occurred, a damage zone may be left in the crystal. Molecular dynamics (MD) simulations were used by Carturla *et al.*[3] to study the isolated cascade structures of B and As implantations into Si at various energies. In their study, As implantations resulted in the formation of large clusters with few isolated defects. For the B implantations, no large clusters were produced but many isolated vacancies and interstitials, along with many small point defect clusters, were formed. This difference in cascade morphology was attributed to the high-mass ion causing a localized melting of the cascade core resulting in an amorphous pocket, whereas in the light ion case, localized melting did not take place and the defects were produced as a result of the early collision phase of the cascade. Diaz de la Rubia also drew the same conclusions in a separate MD study,[4] and some experimental observations using transmission electron microscopy[5,6] (TEM) are also in agreement.

As the ion fluence increases to some critical value, a continuous amorphous layer may be produced within the crystal. The two models for the nucleation of the amorphous phase are the heterogeneous and homogeneous models.

In the heterogeneous model of nucleation, each ion that enters the target produces a separate isolated amorphous zone, and as the fluence increases, the individual zones begin to overlap with each other producing an amorphous layer. This was first suggested and modeled by Morehead and Crowder[7] whose model was based on cylindrical amorphous ion tracks that are produced along the entire range of the ion. While this model is reasonable for high energy heavy ions, it is inadequate when extended to lower energies and lighter ions.

In order to take this problem into account, Gibbons[8] extended the model of Morehead and Crowder. In this modified model, Gibbons suggested that each incoming ion does not necessarily produce an amorphous zone and that instead cascades must overlap with each other in the same region to turn the crystal to amorphous. Although this modified model is an improvement on the Morehead and Crowder model, it still is essentially a two-dimensional model given its modeling of areas (i.e., cylindrical cascades) rather than volumes.

The homogeneous model is based on the ion irradiation not generating discrete zones of amorphous material with each ion but instead the irradiation causes a buildup of defects[9–11] to a point at which the lattice becomes unstable and spontaneously collapses into the amorphous phase. Under this mechanism, the crystalline-to-amorphous transition

[a)]Electronic mail: p.d.edmondson@salford.ac.uk.

 © 2009 American Institute of Physics

Downloaded 24 Aug 2009 to 146.87.0.77. Redistribution subject to AIP license or copyright; see http://jap.aip.org/jap/copyright.jsp

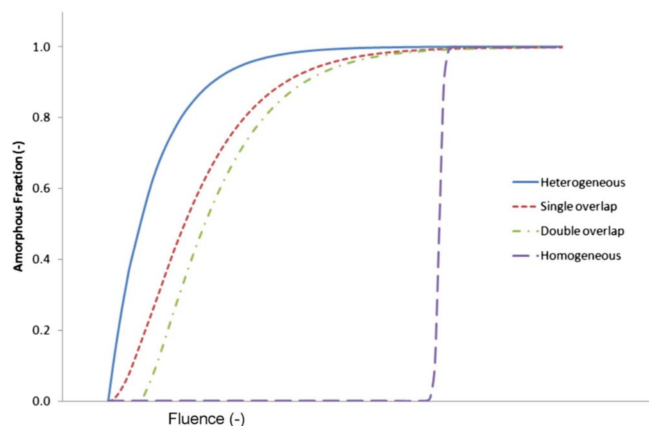

FIG. 1. (Color online) Graph showing the different proposed amorphization mechanisms in silicon: the heterogeneous model, the overlap model, and the homogeneous model.

would be expected to occur over a narrow fluence range. This model is generally accepted to be the operative amorphization mechanism under light ion irradiation.

Figure 1 schematically shows the amorphization curves that would be expected by the Morehead and Crowder heterogeneous model, the Gibbons overlap model, and the homogeneous model. Displacement cross sections have been chosen so that similar ion fluences are required for complete amorphization.

In this paper, we present experimental measurements of ion beam induced amorphization of silicon during irradiation with Si and Xe ions. In order to determine the amorphization mechanism(s), we also present a three-dimensional numerical amorphization model that we have developed. It will be shown that individual ion impacts do not form discrete amorphous zones as previously assumed in literature but instead produce discrete damage regions which must overlap to form amorphous material.

EXPERIMENTAL METHODS

Specimens were prepared from single-side-polished 300 μm thick, *p*-type (boron doped, 80–180 Ω cm) {100} Czochralski silicon wafers by the small angle cleavage technique.[12] In this technique, specimens are produced by first mechanically backpolishing small areas of silicon, 3×5 mm^2, down to a thickness of approximately 100 μm before backscribing along the $\langle 120 \rangle$ direction (18.4° to the $\langle 110 \rangle$ direction). The sample is then cleaved along these scribe lines in order to produce thin silicon strips. A small region of the strip is then front scribed along the $\langle 110 \rangle$ and then a small amount of pressure is applied causing a crack to propagate in the $\langle 110 \rangle$ direction. As the propagating crack approaches the cleaved {120} plane, a triangular based pyramid is formed which is composed of the front surface and the two cleaved sides. It is around this area in which the sample is electron transparent. Wedges that, under an optical microscope, appeared to have a high probability of being electron transparent are then mounted with a $\langle 001 \rangle$ surface normal onto a copper hole grid using a silver epoxy.

The *in situ* irradiations were carried out in a Hitachi H-9000 NAR TEM, operating at 100 keV, located at the IVEM/Tandem facility at Argonne National Laboratory.[13] In this facility, the ion beam is orientated 30° from the microscope axis. The samples were mounted on either a Gatan dual-tilt heating holder or an Oxford Instruments dual-tilt cryogenic stage for the room temperature (300 K) and low temperature (50 K) irradiations, respectively.

As with all experimental techniques, TEM has limitations which must be identified and minimized so that reliable information can be obtained. In the context of the work presented here, the specimen thickness, typically of the order of <0.1 μm for TEM specimens, could result in possible perturbations to the results, i.e., the presence of an additional surface could (by acting as a source or a sink for defects) impede or facilitate the amorphization process. In fact, a study by Williams *et al.*[14] of the amorphization of silicon containing nanocavities during irradiation with self-ions showed that, in this system, amorphization occurs preferentially around the cavities. This was attributed to the fact that as amorphization results in a slight decrease in density (i.e., an increase in volume), it is energetically favorable for this to occur near the surface of the cavity where the substrate is free to expand. An identical consideration also holds for a free surface so that if the presence of the second surface in the *in situ* experiments has any effect, it is likely to be to facilitate amorphization. It is important to note that this artifact, if present, would not affect the major conclusions of this paper.

A second potentially perturbatory effect of *in situ* experiments is the inevitable effect of the electron irradiation that results from the use of the electron microscope. To account for this, the electron beam energy was chosen so as to avoid defect production and minimize the electron beam induced healing of pockets of damage, which is known to occur in silicon.[15,16] In order to reduce electron beam effects even further, during ion irradiations the electron beam was not incident upon the sample except to record images and diffraction patterns. Because the electron beam was only incident upon the sample when recording images and diffraction patterns, the effect of electron beam healing is minimized. In previous experiments, it had been observed that during irradiation with the electron beam incident upon the sample, it was not possible to achieve full amorphization. Although measurements of the amorphous fraction were taken by recording diffraction patterns (as will be discussed later), at low fluences ($\sim 10^{10}$–10^{11} ions cm^{-2}), real images were also recorded under downzone conditions[17] using structure-factor contrast.[18] This has been shown to provide the best conditions and resolution for the imaging of isolated amorphous/damage zones.[17]

The ability to irradiate *in situ* and follow one area is of prime importance in this type of study due to the tendency of zones of damage produced by low-fluence irradiation to recrystallize at low temperatures.[19] Previous works by some of

Downloaded 24 Aug 2009 to 146.87.0.77. Redistribution subject to AIP license or copyright; see http://jap.aip.org/jap/copyright.jsp

the current authors (see, for example, Refs. 19 and 20) have shown that zones of damage may recrystallize at temperatures of as low as 50 °C. It has also been observed during previous experiments that some of the low-fluence damage annealed at room temperature over a period of less than 24 h. This is in contrast to other types of radiation damage, such as dislocation loops and bubbles, which are stable at room temperature.

Before any irradiations were carried out, reference diffraction patterns of the virgin silicon were recorded, on photographic film, at several exposures in the downzone (001) condition using the nanobeam mode of the TEM. This mode alters the lens settings of the microscope in such a way that a much narrower electron beam is produced. By using this mode, small spot sizes of approximately 8 nm in diameter are possible, ensuring that a small sampling region was used throughout the experiments. On wedge-shaped specimens, the small spot size enables the electron beam to sample only the thinner area of the specimen which will be entirely penetrated by the ion beam. This is important as otherwise deeper regions of the specimen not penetrated by the ion beam could be inadvertently sampled. Once the initial diffraction pattern was recorded, the strength of the condenser lens was not altered for subsequent experiments so as to ensure that the number of electrons contributing to the diffraction patterns did not vary during the irradiations for a given exposure time.

During ion irradiation, the ion beam was blanked temporarily at different fluence steps so as to allow for the recording of nanobeam diffraction patterns at that particular ion fluence. At each fluence step, the diffraction pattern was recorded at several exposure times.

The developed photographic negatives were scanned into a personal computer at a resolution of 600 dpi and saved as tiff files. Using Adobe Photoshop CS, a 15 pixel-wide intensity profile was taken across the width of the negative, ensuring that each profile passed through the central beam spot but avoided diffracted beam spots in order to measure the intensity of the amorphous ring as it began to appear with increasing ion fluence. The 15 pixel width was chosen to give a reasonable signal-to-noise ratio.

Data making up the intensity profile were then exported to Microsoft Excel where the background noise was removed and the intensity profile in the region of the amorphous peaks was integrated. After obtaining the integrated intensities for all the fluences, each fluence step intensity was normalized to that of the completely amorphized silicon in order to generate amorphous fraction curves as a function of the ion fluence.

It is believed that this is a valid method to measure the amorphousness of the substrate given that the Si atoms making up the lattice will strongly forward scatter the incident electrons irrespective of their spatial arrangement; thus, as the substrate undergoes the change from crystalline to amorphous, the transmitted electron intensity would transit from the crystalline spots to the amorphous rings *pro-rata* with the number of atoms in each phase. It is thus further, inherently, assumed that the measurement of the amorphous fraction in

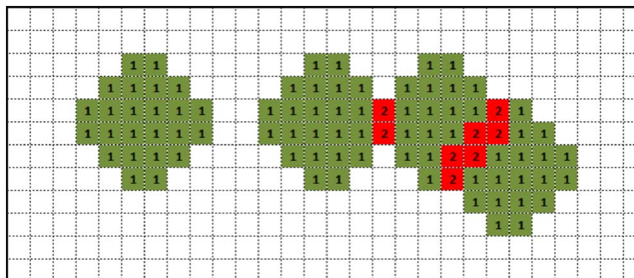

FIG. 2. (Color online) Schematic diagram showing the incremental counting of the numerical model of damage buildup. The "1"s represent a voxel hit once and the "2"s represent voxels hit twice.

the substrate scales linearly with the intensity in the amorphous rings.

NUMERICAL MODEL OF AMORPHIZATION

A simple numerical model to describe the amorphization of silicon due to ion irradiation has been developed. The model requires three inputs for each ion species and irradiation energy: the probabilistic damage distribution as determined from TRIM[21] and the mean radius of damage zones and the number of zones produced per ion as obtained from experimental observations.

The model is very simple and works thus: firstly, the user-defined input file is created, setting up the required parameters. Secondly, the "crystal" into which the ions are to be implanted is set up in the form of an array consisting of numerous voxels with an optimal size of 0.5 nm. The optimal resolution was determined by running calculations at decreasing voxel size until a further resolution resulted in less than 5% change in the amorphization curve.

For the "implantation" procedure that follows, the x and y coordinates of a cascade center are chosen (pseudo)randomly and the z coordinate is chosen via a weighted random process that scales the probability of a particular depth being chosen using the damage distribution for the ion and energy in question from SRIM. After the cascade occurrence point (the position at which the "ion" has come to rest) has been determined, a cascade sphere is centered about these coordinates using the mean radius determined from the experimental observations. The program then checks all the voxels to determine which voxels are contained within the cascade volume. Those voxels that have their center contained within the cascade volume, and hence have been determined to have been "hit," have their counter incremented by 1. This is schematically shown in two dimensions in Fig. 2 in which we also show the regions in which zones have overlapped. After the required ion fluence has been reached, the data are written to a file. In this way the program keeps a tally of the number of times that a voxel has been included within a cascade, i.e., the number of "hits."

RESULTS AND DISCUSSION

An example of the diffraction patterns obtained during irradiation with 400 keV Xe^+ is shown in Fig. 3. It can be seen in this figure that at zero fluence [virgin sample, Fig. 3(a)], only the diffraction spot characteristics of the crystal-

Downloaded 24 Aug 2009 to 146.87.0.77. Redistribution subject to AIP license or copyright; see http://jap.aip.org/jap/copyright.jsp

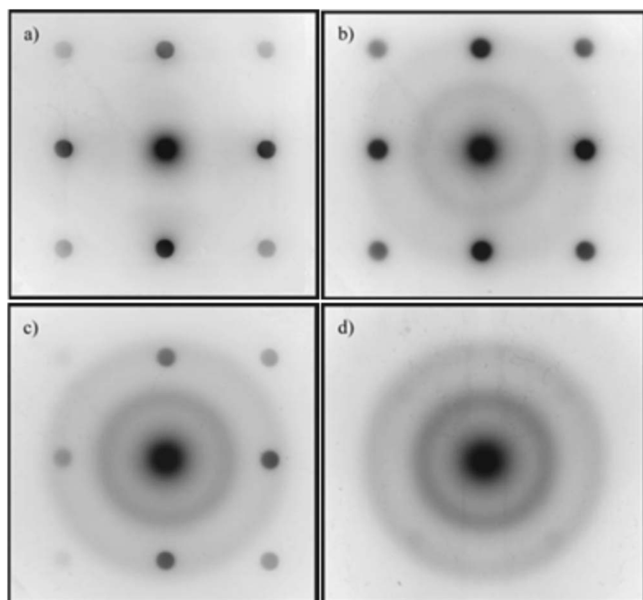

FIG. 3. Example of diffraction patterns taken during 400 keV Xe, room temperature, *in situ* ion irradiation: (a) virgin, (b) 8×10^{13} ions cm^{-3}, (c) 1×10^{14} ions cm^{-3}, and (d) 2×10^{14} ions cm^{-2}. During the experiments, more data were recorded in order to produce an amorphization curve.

line phase are visible. As the ion fluence is increased, halos indicative of the amorphous phase begin to appear with the crystalline spots still visible, demonstrating the coexistence of both the crystalline and amorphous phases in the substrate [Figs. 3(b) and 3(c)]. At high fluence, the crystalline spots are no longer observable and only the halos remain, signifying that the crystal has been rendered completely amorphous [Fig. 3(d)]. By the analysis of the halos through this transition from crystalline-to-amorphous material, followed by normalization to the fully amorphous results, it is possible to obtain a graph that shows the percentage of amorphous content in the substrate as a function of the ion fluence as shown in Fig. 4 for the case of the Xe irradiations. It can be seen from this graph that in both low and room temperature cases there is an "S" shape to the amorphization curves. It can also be seen that the low temperature irradiation amorphizes the sample at a lower fluence than the room temperature one.

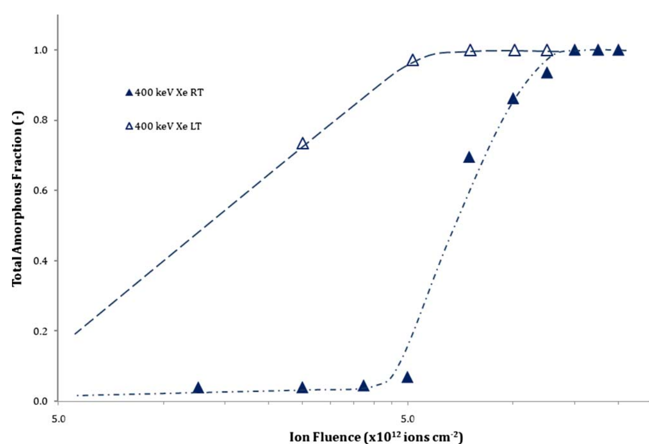

FIG. 4. (Color online) Graph showing the amorphization curves as obtained from room temperature and low temperature (50 K), 400 keV Xe^+ irradiations.

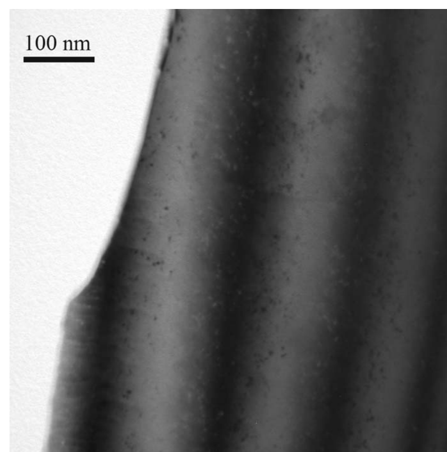

FIG. 5. Micrograph showing damage zones resulting from low-fluence ($\sim1\times10^{11}$ ions cm^{-2}) 400 keV Xe ion irradiation as imaged under downzone structure-factor conditions in the TEM.

This is to be expected as recombination effects will be either prevented or significantly diminished at low temperature. The results from the Si irradiation showed a similar overall behavior, although the onset of amorphization occurred at higher fluences—as would be expected with the lower damage production rate of an ion of lighter mass.

In addition to the diffraction patterns recorded throughout the irradiations, images of the damage caused by the ions at low fluences, where cascade overlap is minimal ($\sim10^{11}$ ions cm^{-2}), were recorded under downzone conditions[17] using structure-factor contrast.[18] An example of these images is shown in Fig. 5. It can be seen from this image that the damage is in the form of spatially isolated damage zones of contrast produced by the ions at these low fluences. These have been referred to as amorphous zones in literature.[20,22] During the *in situ* observations, it can be seen that as the ion fluence increases, these zones begin to overlap with each other up to an ion fluence at which the extinction fringes characteristic of the crystalline phase disappear. It should be noted, however, that it is not possible to observe the amorphization of the sample during ion irradiation as the presence of the electron beam hinders the amorphization. For this reason, the electron beam was generally off during our experiments.

Shown in Fig. 6 are the results obtained by the numerical model for the Xe irradiation, demonstrating the variation in the curves for the different numbers of overlaps required to produce amorphous material in the crystal. As the number of overlaps required to render the crystal amorphous is increased, the onset of amorphization shifts to higher fluences, and the gradient of the curve becomes steeper.

Shown in Figs. 7 and 8 are the graphs of the simulations and the experiments for both the Xe and Si irradiations. As can be seen from the graphs (now in a linear plot), in both the Xe and Si cases, the low temperature irradiations produce the amorphous phase at a lower fluence than the respective room temperature irradiations. At lower temperatures, the mobility of defects formed within the collision cascade volume is substantially reduced and, as such, the damage can be expected to be quenched into a larger volume producing

Downloaded 24 Aug 2009 to 146.87.0.77. Redistribution subject to AIP license or copyright; see http://jap.aip.org/jap/copyright.jsp

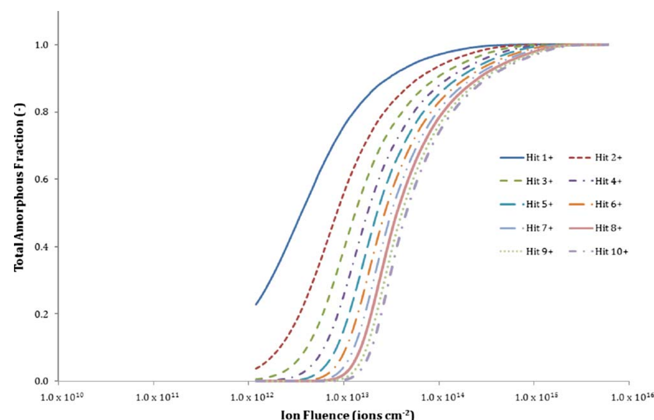

FIG. 6. (Color online) Graph showing the results of the numerical model.

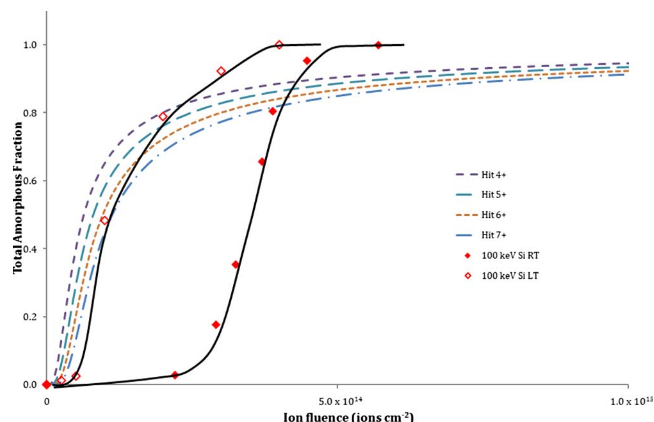

FIG. 8. (Color online) Graph showing the results of the experimental (at both room temperature and 50 K) and simulated amorphizations of silicon as a result of 100 keV Si^+ irradiation. Note that the graph is now shown with a linear abscissa for clarity.

more stable damage. During the room temperature irradiations, the mobility of some defects will be sufficiently high to permit both recombination and loss of defects from the cascades volume (dynamic annealing).

It can also be seen from Figs. 7 and 8 that the form of the curves in the simulations is closer to the low temperature experimental results than those for the room temperature results. This can be attributed primarily to the dynamic annealing that occurs in the room temperature experiments—as discussed previously. In addition, the cascade volume for the numerical model is taken from the mean cascade radius as obtained by measurements of the zones of contrast observed in the TEM. This, obviously, does not account for the variation in sizes of cascade volumes that physically occurs and may be expected to provide a minor perturbation in the calculated curves.

For the lower temperature Xe irradiation, it can be seen that the experimentally obtained data fit best with the "hit 2+" or "hit 3+" curve. Although there is only one data point in this region, the point is significantly far enough from the "hit 1+" curve to state with some degree of confidence that heterogeneous nucleation of the amorphous phase does not generally occur and that the zones produced by each individual ion must overlap with each other, on average, between one and two times before rendering the overlap region amorphous. As the amorphous fraction increases, it can be seen from Fig. 7 that the experimental data begin to increase at a much faster rate than the simulated curves. If we now consider the room temperature Xe irradiation, it can be seen that the numerical model results do not agree with the experimentally obtained data. The explanation for this discrepancy is due to dynamic annealing.

If we now turn to the Si irradiations, it can be seen that for the low temperature irradiations the experimental data lie somewhere in between the "hit 4+" and "hit 7+" curves with the same characteristic as the Xe low temperature case with the curve rapidly increasing at higher fluences. The rapid increase in amorphization of the experimental results compared to the overlap model is attributed to the injection of point defects into regions outside the cascade volume during each collision cascade, i.e., the point defects are not all contained within the defected region imaged by the TEM. As the ion fluence increases, the point defect concentration in regions unperturbed by collision cascades increases to a concentration at which the lattice collapses from the defected crystalline phase into the amorphous phase, thus resulting in a rapid increase in the fraction of amorphous material observed as a function of the ion fluence.

Again the room temperature case does not agree with any of the simulated curves. In both the Si and Xe cases, the room temperature irradiations are closer somewhat to that expected during homogeneous nucleation of the amorphous phase, although the amorphization curves do not exhibit a purely homogeneous nature. This is possibly due to the increased diffusion of defects from the collision cascade during the relaxation phase of the thermal spike. Again, this tends toward an increase in the concentration of point defects that will collapse at a critical concentration. At room temperature, this is the dominant mechanism with the overlap mechanism having a less pronounced role in the amorphization of silicon.

These results clearly indicate that neither in the light nor heavy ion case is amorphous material generally produced by single ion impacts (although there will be a statistical probability that in some cases the energy deposited into the cas-

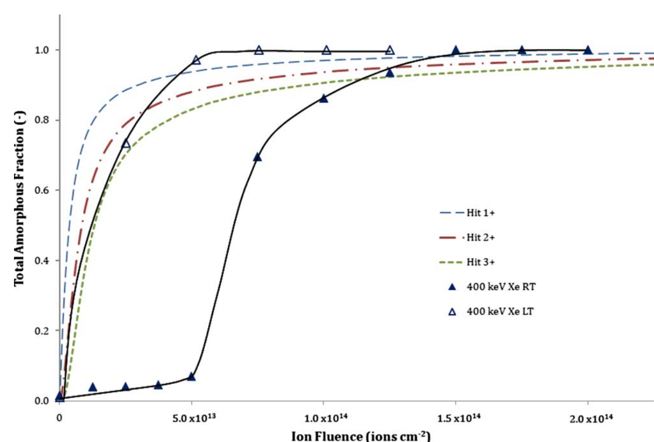

FIG. 7. (Color online) Graph showing the results of the experimental (at both room temperature and 50 K) and simulated amorphization of silicon as a result of 400 keV Xe^+ irradiation. Note that the graph is now shown with a linear abscissa for clarity and the dashed line is to guide the eye only.

Downloaded 24 Aug 2009 to 146.87.0.77. Redistribution subject to AIP license or copyright; see http://jap.aip.org/jap/copyright.jsp

cade volume would be sufficient to produce an amorphous zone). This is in agreement with other recent experimental observations on the amorphization of silicon during molecular ion[23] and ion cluster[24] irradiations. This is in contrast to the work performed in the late 1970s/early 1980s by Thomson and co-workers (see, for example, Refs. 25–27), although work performed by Donnelly and Birtcher[2] has more recently shown that the thermal spike model proposed by Walker and Thomson to cause localized melting within the cascade, followed by quenching in the amorphous structure is not a feasible mechanism for substrates having a bulk density of approximately ≤ 7 g cm^{-3}. In the recent molecular and cluster ion work, it was shown that the damage created by each single molecule/cluster "particle" increased with increasing numbers of atoms in the molecule/cluster. This was true for both low and room temperature irradiations and was attributed to the spatial overlapping of the collision cascades produced by the atoms forming the molecule/cluster. During the cluster ion irradiations at room temperature, it was discovered that clusters containing five gold atoms did not produce amorphous material within the collision cascade, yet clusters containing seven gold atoms did produce amorphous material. This is in clear agreement with the results presented here and it can be stated that the zones observed following individual ion impacts are thus not generally amorphous. The question that then arises is what is the nature of the damaged material in these zones. It is thus far clear that the damage contained within the zones may consist of anything from Frenkel pairs to fully amorphous material in any combination.

In order to determine the nature of the damage contained within the cascades, it is useful to consider known types of damage in Si that have been imaged in the TEM and to compare them with the contrast observed in the current experiments. Known damage configurations observable in the TEM are interstitial clusters, vacancy clusters, rod-and ribbonlike defects such as {113}s, stacking faults and microtwins, dislocation loops (full, partial, or faulted), and bubbles and voids. Note that isolated interstitials and vacancies are not visible in our experiments and precipitates have not been included as only Xe and Si implantations are under consideration here.

In Fig. 9, TEM images of rod- and ribbonlike defects [Fig. 9(a)], dislocation loops [Fig. 9(b)], under- and overfocussed bubbles [Figs. 9(c) and 9(d)], stacking faults, and microtwins [Figs. 9(e) and 9(f)] are shown in their optimum imaging conditions. Examining and comparing the images shown in this figure and those of the zones shown in Fig. 5, it can be quickly determined that the zones observed following single ion impacts do not exhibit contrast similar to those in Fig. 9; thus, the zones do not contain any of these damage configurations. This is not unexpected as these defects are stable defects formed following various implantation and annealing schemes.

Now looking at the images shown in Fig. 10 we can see that in certain imaging conditions (downzone structure-factor contrast), the damage zones produced by low- fluence irradiation [Fig. 10(a)] are similar to the regions of contrast produced by interstitial clusters formed during high fluence im-

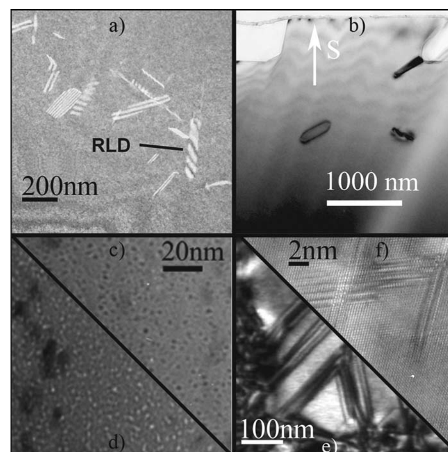

FIG. 9. Image showing the various types of defects produced during ion irradiation in silicon as imaged in the TEM: (a) rod- and ribbonlike defects, (b) dislocation loops (full and partial), [(c) and (d)] overfocussed and underfocussed bubbles, (e) stacking fault tetrahedral, and (f) microtwins.

plantation of helium [Fig. 10(b)]. However, by tilting the specimen by a few degrees ($\sim 10°$), as shown in Figs. 10(c) and 10(d), the contrast resulting from the damage zones is extinguished, whereas the contrast from the interstitial clusters is still strongly present, arising as it does from diffraction contrast resulting from the strain surrounding the interstitial clusters. It is thus possible to state with confidence that the damage zones observed are most likely not solely interstitial in nature.

It is, therefore, clear that the contrast (under appropriate imaging conditions) for all the defects described above differs significantly from that due to the damage zones presented in this work, i.e., the damage zones do not contain defects introducing strain into the lattice, nor are they large vacancy-type agglomerations such as bubbles. The configuration of defects contained within the damage zones most

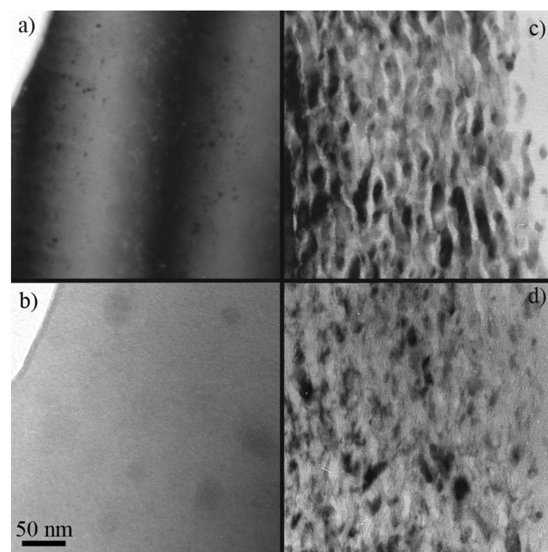

FIG. 10. Image showing damage zones produced by single ion impacts in both the downzone structure-factor condition (a) and in the weak-beam bright-field condition (b); and interstitial clusters formed by high fluence helium irradiation in the downzone structure-factor condition (c) and in the weak-beam bright-field condition (d).

Downloaded 24 Aug 2009 to 146.87.0.77. Redistribution subject to AIP license or copyright; see http://jap.aip.org/jap/copyright.jsp

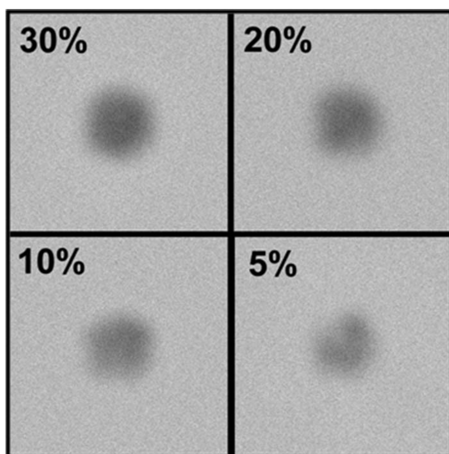

FIG. 11. Simulation results from JEMS for the *I-V* pair in different defect concentrations. It can be seen from this figure that defect configurations below that of the amorphous configuration (25%) exhibit structure-factor contrast.

likely consists of interstitials and vacancies in various combinations and concentrations that do not induce significant strain into the lattice (i.e., relatively equal numbers). One possible defect configuration candidate involving equal numbers of vacancies and interstitials is the interstitial vacancy pair or bond defect. This defect, first discovered in computer simulations by Tang *et al.*,[28] has been shown during MD simulations to be formed during the ballistic process that occurs during ion implantation.[29] As yet there have been no confirmed experimental observations of this defect, a fact that has been attributed to its fourfold coordination ensuring that it is not easily observed by techniques such as deep-level transient spectroscopy and electron paramagnetic resonance. As the localized concentration of the *I-V* pair increases to approximately 25%, the radial pair distribution of the crystal becomes indistinguishable from that of amorphous silicon resulting from quenching from the melt.

In order to test the credibility of the suggestion that the *I-V* pair may be the defect responsible for the regions of contrast observed in the TEM, image simulations were performed using the JEMS software package [a modified version of EMS (Ref. 30) designed to operate on all computer platforms] using clusters of *I-V* pairs with concentrations varying from 5% to 30% embedded in a crystalline matrix. The results of these simulations are shown in Fig. 11. It can be seen in these simulated images that it is possible to produce regions of contrast using the structure-factor conditions used from zones containing damage concentrations ranging from fully amorphous (30%) down to relatively low concentrations (5%). This contrast closely mirrors the types of contrast observed in our experiments to result from single ion impacts and thus provides some supporting evidence for our suggestion that the defects contained within our damage zones may consist (fully or partially of *I-V* pairs). However, given than the *I-V* pair has thus far only been observed in computer simulations, we seek an experimental technique to be used in our specimens that would uniquely serve to indicate the presence of *I-V* pairs.

Overall this work has demonstrated that silicon does not amorphize either by a single hit, direct impact, nucleation process or by a purely homogeneous nucleation process for the ion masses and energies discussed here, but by a damage zone overlap process that is assisted by a homogeneous process at high damage levels. During this process, the collision cascades overlap with each other forming higher levels of stable damage that, for a given number of overlaps, produces amorphous material. At a certain level of damage, our results suggest that regions that have not been hit by the required number of cascades may spontaneously collapse into the amorphous phase through a homogeneous-type nucleation process that occurs as a result of the injection of isolated defects being produced outside of the denser cascades that are imaged in the TEM—in essence, both heterogeneous and homogeneous nucleations of the amorphous phase occur.

CONCLUSIONS

The buildup of amorphous Si by heavy and light ion irradiation at both room and low temperatures has been measured by electron diffraction during *in situ* ion irradiation in a TEM. In addition, a numerical model has been developed in which the experimentally observed statistical information on the zones of contrast produced in the TEM is used as input data. The comparison of the experimentally observed damage accumulation with the simulated buildup curves demonstrates that Si is not generally amorphized by direct individual single ion impacts, but, on average, by a localized multiple-hit process. We conclude that the damage configuration of the zones of contrast produced by individual ions is the result of interstitial, vacancies, and *I-V* pairs in various combinations, configurations, and concentrations within the collision cascade.

ACKNOWLEDGMENTS

Two of the authors (P.D.E. and S.E.D.) would like to thank Argonne National Laboratory for funding during extended stays at Argonne. P.D.E. and D.J.R. would also like to thank the U.K. Engineering and Physical Sciences Research Council for funding. The authors would also like to give special thanks to K.J. Abrams, A.S. Gandy, and M.-F. Beaufort for the provision of TEM images, L. Pelaz and L.A. Marques for providing the atomic configuration files for the TEM image simulations, and W. Weber for useful discussions.

[1]J. A. Brinkman, J. Appl. Phys. **25**, 961 (1954).
[2]S. E. Donnelly and R. C. Birtcher, Philos. Mag. A **79**, 133 (1999).
[3]M.-J. Carturla, T. Díaz de la Rubia, and L. A. Marqués, Phys. Rev. B **54**, 16683 (1996).
[4]T. Diaz de la Rubia, Nucl. Instrum. Methods Phys. Res. B **120**, 19 (1996).
[5]L. M. Howe and M. H. Rainville, Nucl. Instrum. Methods Phys. Res. B **182-183**, 143 (1981).
[6]L. M. Howe and M. H. Rainville, Nucl. Instrum. Methods Phys. Res. B **19/20**, 61 (1987).
[7]F. F. Morehead and B. L. Crowder, Radiat. Eff. **6**, 27 (1970).
[8]J. F. Gibbons, Proc. IEEE **60**, 1062 (1972).
[9]L. T. Chadderton, Radiat. Eff. **8**, 77 (1971).
[10]M. L. Swanson, J. R. Parsons, and C. W. Hoelke, Radiat. Eff. **9**, 249 (1971).
[11]F. L. Vook and H. J. Stein, Radiat. Eff. **2**, 23 (1969).
[12]J. P. McCaffrey, Ultramicroscopy **38**, 149 (1991).
[13]C. W. Allen, L. L. Funk, E. A. Ryan, and S. T. Ockers, Nucl. Instrum.

Downloaded 24 Aug 2009 to 146.87.0.77. Redistribution subject to AIP license or copyright; see http://jap.aip.org/jap/copyright.jsp

Methods Phys. Res. B **40/41**, 553 (1989).
[14]J. S. Williams, X. Zhu, M. C. Ridgway, M. J. Conway, B. C. Williams, F. Fortuna, M. O. Ruault, and H. Bernas, Appl. Phys. Lett. **77**, 4280 (2000).
[15]I. Jencic, M. W. Bench, I. M. Robertson, and M. A. Kirk, J. Appl. Phys. **78**, 974 (1995).
[16]I. Jencic and I. M. Robertson, J. Mater. Res. **11**, 2152 (1996).
[17]M. W. Bench, D. K. Tappin, and I. M. Robertson, Philos. Mag. Lett. **66**, 39 (1992).
[18]M. F. Ashby and L. M. Brown, Philos. Mag. **8**, 1649 (1963).
[19]P. D. Edmondson, R. C. Birtcher, V. M. Vishnyakov, P. Lopez, L. Pelaz, L. A. Marques, and S. E. Donnelly, J. Phys.: Conf. Ser. **26**, 284 (2006).
[20]S. E. Donnelly, R. C. Birtcher, V. M. Vishnyakov, and G. Carter, Appl. Phys. Lett. **82**, 1860 (2003).
[21]J. F. Ziegler, J. P. Biersack, and U. Littmark, *The Stopping and Ranges of Ions in Solids* (Pergamon, Oxford, 1985).
[22]M. O. Ruault, J. Chaumont, J. M. Penisson, and A. Bourret, Philos. Mag. A **50**, 667 (1984).
[23]A. I. Titov, S. O. Kucheyev, V. S. Belyakov, and A. Y. Azarov, J. Appl. Phys. **90**, 3867 (2001).
[24]B. Canut, M. Fallavier, O. Marty, and S. M. M. Ramos, Nucl. Instrum. Methods Phys. Res. B **164–165**, 396 (2000).
[25]D. A. Thompson, Radiat. Eff. **56**, 105 (1981).
[26]D. A. Thompson and R. S. Walker, Nucl. Instrum. Methods **132**, 281 (1976).
[27]D. A. Thompson and R. S. Walker, Radiat. Eff. **36**, 91 (1978).
[28]M. Tang, L. Colombo, J. Zhu, and T. Diaz de la Rubia, Phys. Rev. B **55**, 14279 (1997).
[29]D. M. Stock, B. Weber, and K. Gartner, Phys. Rev. B **61**, 8150 (2000).
[30]P. A. Stadelmann, Ultramicroscopy **21**, 131 (1987).

Downloaded 24 Aug 2009 to 146.87.0.77. Redistribution subject to AIP license or copyright; see http://jap.aip.org/jap/copyright.jsp